

Chapter 3

Crystal structures of dodecaborides: complexity in simplicity

Nadezhda B. Bolotina^{a,*}, Alexander P. Dudka^{a,b},
Olga N. Khrykina^{a,b}, and Vladimir S. Mironov^a

^a*Shubnikov Institute of Crystallography of the Federal Scientific Research Center
"Crystallography and Photonics" of the Russian Academy of Sciences, Leninsky Prospekt
59, 119333 Moscow, Russia*

^b*Prokhorov General Physics Institute, Russian Academy of Sciences, Vavilova str. 38,
119991 Moscow, Russia*

*E-mail address: bolotina@ns.crys.ras.ru

Abstract

Analysis of the intriguing physical properties of the dodecaborides, RB_{12} , requires accurate data on their crystal structure. We show that a simple cubic model fits well with the atomic positions in the unit cell but cannot explain the observed anisotropy in the physical properties. The cooperative Jahn-Teller (JT) effect slightly violates the ideal metric of the cubic lattice and the symmetry of the electron density distribution in the lattice interstices. Theoretical models of the JT distortions of the boron framework are presented. Their correspondence to the electron-density distribution on the maps

Rare-Earth Borides

Dmytro S. Inosov (ed.)

Copyright © 2020 by Jenny Stanford Publishing Pte. Ltd.

www.jennystanford.com

2 | Chapter 3 Crystal structures of dodecaborides: complexity in simplicity

of Fourier syntheses obtained using x-ray data and explaining the previously observed anisotropy of conductive properties is demonstrated. The effect of boron isotope composition on the character of the lattice distortions is shown. We also discuss the application of the Einstein model for cations and the Debye model for the boron atoms to describe the dynamics of the crystal lattice.

3.1 Introduction

There is a wide variety of borides formed by different-in-shape boron polyhedra in combination with most metals, resulting in a metal-to-boron ratio ranging from 4:1 to 1:66. A highly symmetrical $Fm\bar{3}m$ structure of the uranium dodecaboride UB_{12} was the first one of this type [1]. A unit cell of the cubic lattice with the lattice constant $a = 7.473 \text{ \AA}$ contains four UB_{12} formula units. The metal atoms occupy centers of truncated B_{24} octahedra with boron atoms at each of their 24 vertices. Every boron atom is bonded to two metal atoms and to five other boron atoms. The metal and boron atoms are in positions $4a \{0, 0, 0\}$ and $48i \{0.5, y, y\}$ of the $Fm\bar{3}m$ group, respectively, with y close to $1/6$. This compound may also

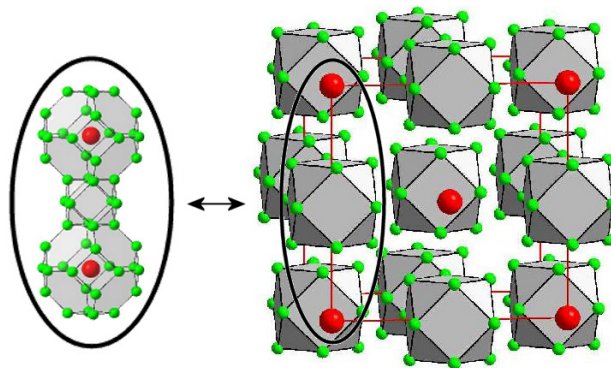


Figure 3.1 Left: two metal-centered truncated B_{24} octahedra of the UB_{12} -type structure, connected by one empty B_{12} cubooctahedron. Right: The same structure presented as a NaCl-type structure. The metal atoms (large spheres) alternate in a checkerboard pattern with the B_{12} cubooctahedra.

be described in terms of the NaCl-type structure, in which metal atoms and regular B_{12} cuboctahedra occupy the Na and Cl positions, respectively, resulting in a face-centered cubic (fcc) structure shown in Fig. 3.1.

Three years later, the isomorphous ZrB_{12} was prepared and studied [2]. Six UB_{12} -type structures of the rare-earth dodecaborides RB_{12} ($R = Y, Dy, Ho, Er, Tm, Lu$) were determined [3] based on the x-ray powder diffraction data. The authors of Ref. [4] reported the cubic symmetry after examination of a powder ScB_{12} sample. The cubic structure of YB_{12} was later confirmed on single crystals [5], but a single crystal of ScB_{12} studied in the same work [5] was determined as tetragonal $I4/mmm$, with unit-cell parameters $a_{tet} \approx 5.22 \text{ \AA}$, $c_{tet} \approx 7.35 \text{ \AA}$ that could be transformed to pseudo-cubic: $a = b = a_{tet}\sqrt{2} \approx 7.38 \text{ \AA}$, $c = c_{tet} \approx 7.35 \text{ \AA}$. All the above findings were summarized in a review article [6]. A more recent review [7], which was mainly devoted to magnetic, superconducting, and other physical properties of rare-earth dodecaborides, began by describing the dodecaboride structure and by presenting structural information on RB_{12} with $R = Tb-Lu$ from the second half of the lanthanide series supplemented with YB_{12} and ZrB_{12} . Background information on higher borides of rare earths, including dodecaborides, has been summarized in [8]. It is worth noting that the rare-earth dodecaborides RB_{12} differ from other higher borides RB_n , $n > 12$. All the dodecaborides, except YbB_{12} , are good metals similar to RB_6 and RB_4 , whereas RB_n with $n > 12$ are insulators. Both B_{12} cuboctahedra and icosahedra are electron-deficient by two electrons. The trivalent rare-earth atoms can supply three electrons, so there is one excess conduction electron per unit cell. The only exception is the narrow-gap semiconductor YbB_{12} , known also as a Kondo insulator, where Yb takes an intermediate valence. The summary table of structural, electronic and magnetic characteristics of the dodecaborides of the UB_{12} type different in isotope boron composition is presented in Ref. [9]. In addition to the rare-earth dodecaborides $TbB_{12}-LuB_{12}$ mentioned above, this table contains ZrB_{12} , HfB_{12} , pseudo-cubic ScB_{12} , GdB_{12} synthesized under high pressure [10] as well as dodecaborides of heavy metals ThB_{12} , UB_{12} , NpB_{12} , PuB_{12} and several solid solutions $R1_xR2_{1-x}B_{12}$ of the UB_{12} type. In the same arti-

4 | Chapter 3 Crystal structures of dodecaborides: complexity in simplicity

cle [9], the lattice constants of RB_{12} as well as the B-B distances in and between the B_{12} cuboctahedra versus ionic radii of the metal atoms are plotted and discussed. A large amount of the reference data on the structures and properties of higher borides, including dodecaborides RB_{12} , is contained in the overview chapter of a recent PhD thesis [11]. Metal dodecaborides MB_{12} attract particular interest as multifunctional materials. For instance, in contrast to conventional superhard materials like diamond, which are insulators or semiconductors, many dodecaborides are superhard compounds with high electrical conductivities that can be used as conductors at extreme conditions [12].

Owing to the simple cubic structure, dodecaborides are convenient objects for studying physical properties of the metal atoms possessing relative freedom in the large B_{24} cavities of the boron framework. There is a large number of publications on the physical properties of dodecaborides. Their crystal structures, however, have not been studied in such detail and are almost not studied at low temperatures (the ZrB_{12} structure at 140 K [13] is a rare exception), although low-temperature physical properties often reveal features that require explanations based on the crystal structure. Moreover, clear explanations are not always easy to obtain in the framework of a simple cubic model. For example, in Refs. [14, 15], linear thermal expansion coefficients α of RB_{12} single crystals, $R = Y, Ho, Er, Tm, Lu$, were measured in the temperature range of 5–300 K. The values of the coefficients at low temperatures varied nonlinearly for all the compounds studied. The nonlinear $\alpha(T)$ dependencies had two minima, sometimes negative in magnitude. Two temperature intervals with negative thermal expansion (NTE) were found for LuB_{12} crystals: the first one was 60–130 K with a minimal negative at 90 K and the second one was 10–20 K with a minimum at 12 K. One NTE interval 50–70 K was revealed for YB_{12} with a negative minimum near 60 K whereas the second minimum at 15 K was close to zero but positive.

The relationship between anomalies of the thermal expansion and crystal structure of the dodecaborides is poorly understood so far. Until recently, published data on the observed anomalies of the RB_{12} structure was actually limited to discussions about observed disordering of the metal atoms near the $4a$ position of the $Fm\bar{3}m$

group [16, 17] and to a short report on a small tetragonal distortion of the LuB_{12} lattice at temperatures below 150 K [18], which was discovered in the analysis of thermal expansion using x-ray data. Reports of a tetragonal distortion of the dodecaboride lattice even at room temperature appeared before, but they only concerned ScB_{12} and Sc-containing solid solutions $\text{Sc}_{1-x}\text{R}_x\text{B}_{12}$ ($R = \text{Y}, \text{Zr}$) [5, 12, 19, 20]. As noted in [20], the origin of the transformation from cubic to tetragonal structure in ScB_{12} is unclear. The influence of the size of scandium is not obvious, as the radius of scandium is located within the limits of atomic radii of metals that form cubic RB_{12} phases. The cell parameters of known dodecaborides are graphically presented in [20] as functions of their d , $4f$, or $5f$ metal radii. All data fit on three straight lines with an individual slope for each group of elements. Yttrium, gadolinium and thorium dodecaborides that finish the corresponding series have almost identical radii but considerably different lattice constants. The d -elements form the Hf–Zr–Sc–Y line with intermediate Sc which enters into the composition of the tetragonal ScB_{12} structure. Structural stability and physical properties of MB_{12} containing transition-metal elements ($M = \text{Sc}, \text{Y}, \text{Zr}, \text{Hf}$) were studied [12] using first-principles calculations supplemented with the x-ray diffraction experiments for ScB_{12} and YB_{12} . The tetragonal $I4/mmm$ structure was predicted to be the thermodynamic ground state of ScB_{12} and a metastable state of YB_{12} , ZrB_{12} , and HfB_{12} . Tetragonal ScB_{12} was shown to transform reversibly into the cubic $Fm\bar{3}m$ symmetry group at 510 K, which corresponded to the thermodynamic ground state of YB_{12} , ZrB_{12} , and HfB_{12} at room temperature. The temperatures of the phase transition between tetragonal and cubic phases of the yttrium and zirconium dodecaborides could be lower than 100 K as predicted in [12].

Neutron diffraction measurements have revealed that HoB_{12} , TmB_{12} and ErB_{12} have incommensurate magnetic structures [21–23]. The complex magnetic structure of these materials seems to result from the interplay between the RKKY and dipole-dipole interactions. Strong frustration of an antiferromagnetic order in the fcc symmetry of the dodecaborides could also play an important role.

3.2 Cooperative Jahn-Teller effect as a driving force behind structural instability in dodecaborides

The origin of small structural distortions in RB_{12} dodecaborides, which distinctly manifest in the background of an almost unchangeable basic cubic structure of the robust boron network, is a challenging and intriguing problem. In most of the works on rare-earth dodecaborides RB_{12} , discussion of structural instability is usually based on the two main points: (a) the boron network is rigid and undistorted, (b) the dimension of the B_{24} cavity is oversized with respect to the central metal ion R ; this results in a rattling character of thermal vibrations of the metal atoms R in the cavities [9, 17, 24–26]. According to this approach, at low temperatures some fraction of the metal ions shifts from the central position in the B_{24} cages to form a cage-glass state [24–27]. These displacements may be caused by lattice defects such as impurities and boron vacancies. These models were extensively used in the analysis of low-temperature structural and magnetic characteristics of RB_{12} compounds [24–27].

However, as will be shown below, the basic assumptions of these models need some revision, since they do not take into account some important features of the electronic structure of the RB_{12} dodecaborides and their structural units. Namely, apart from displacements of R atoms in the oversized B_{24} cages, low-temperature lattice distortions in RB_{12} may originate from intrinsic structural instability of B_{12} cuboctahedra related to the JT effect. This point can be best illustrated for isolated B_{12} units. Similarly to other high-symmetry molecules, such as B_{12} icosahedra in boron and higher metal borides [28, 29], the cuboctahedral boron clusters B_{12} may have an orbitally degenerate ground state resulting in JT distortions of the regular cubic structure. In terms of molecular orbitals (MOs), the orbital degeneracy of the ground state is associated with partial electron occupation of the highest occupied molecular orbital (HOMO) of B_{12} , which is represented by triply degenerate MOs of a t -type symmetry (Fig. 3.2).

Essentially, the character of the JT distortion depends on the electric charge of the B_{12} clusters. In an electrically neutral $[B_{12}]^0$

3.2 Cooperative Jahn-Teller effect as a driving force behind structural instability in... 7

cluster, the HOMO accommodates two electrons (t^2 configuration); in negatively charged clusters $[B_{12}]^{n-}$ ($n = 1-4$), the number m of t -electrons in HOMO increases from three to six (Fig. 3.3). Four electronic configurations t^m with $m = 2-5$ produce a triply degenerate many-electron ground T -state [Fig. 3.3(a-d)] This implies that neutral $[B_{12}]^0$ cluster and charged $[B_{12}]^{n-}$ clusters ($n = 1, 2, 3$) are JT-active systems, which would tend to distort the cubic structure, except the $[B_{12}]^{4-}$ cluster with fully occupied HOMO (t^6 configuration), which has a nondegenerate ground state and thus is not JT-active [Fig. 3.3(e)]. For JT systems with the T -type ground state, the character of distortions is determined by two active vibrational modes of e and t_2 symmetry; such situation is referred to as the $T \times (e + t_2)$ Jahn-Teller problem [30]. In this case, depending

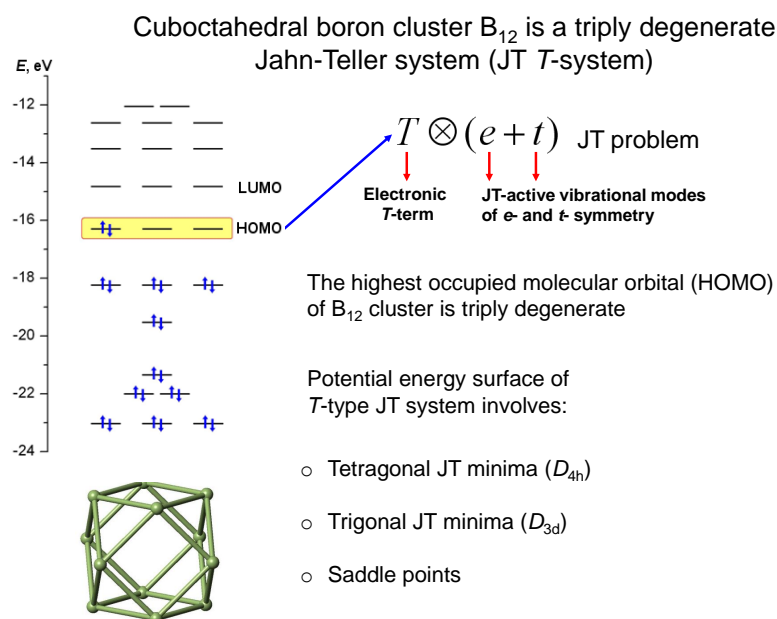


Figure 3.2 On the origin of the Jahn-Teller effect in isolated cuboctahedral B_{12} clusters in RB_{12} compounds. The highest occupied molecular orbital (HOMO) is triply degenerate. Partial population of the HOMO orbitals with electrons produces a triply degenerate many-electron ground T -state, which leads to Jahn-Teller distortions.

8 Chapter 3 Crystal structures of dodecaborides: complexity in simplicity

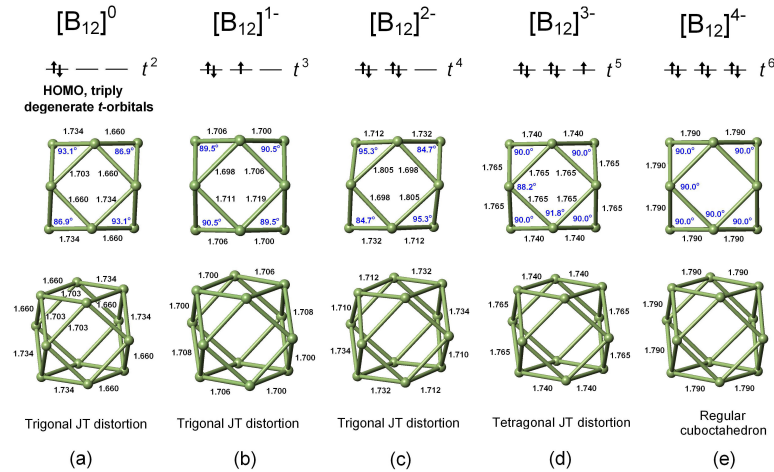


Figure 3.3 Molecular structure of neutral and negatively charged isolated $[B_{12}]^{n-}$ clusters ($n = 0-4$) obtained from DFT geometry-optimization calculations [27]. The optimized structures correspond to the deeper local JT minima of the corresponding charged cluster. Principal atomic distances (\AA) and bond angles are indicated.

on the ratio between the strength of the e and t_2 electron-vibronic couplings, three types of minimum points on the ground-state potential energy surface can occur: trigonal (D_{3d}), tetragonal (D_{4h}) and orthorhombic (D_{2h}) points (Fig. 3.2) [30].

More quantitative information on the amplitude and type of the JT distortions has been obtained from density functional theory (DFT) calculations for the neutral cluster $[B_{12}]^0$ and negatively charged $[B_{12}]^{n-}$ clusters ($n = 1-4$) [27]. Calculated structures of $[B_{12}]^{n-}$ ($n = 0-4$) clusters resulting from the DFT geometry optimization are shown in Fig. 3.3. These results indicate that the JT-active clusters $[B_{12}]^{n-}$ ($n = 0-3$) are slightly distorted cuboctahedra. The character of JT distortions depends strongly on the charge of the cluster: the neutral cluster and charged clusters with $n = 1, 2$ exhibit trigonal type of JT distortions, while the $[B_{12}]^{3-}$ cluster shows tetragonal JT distortion. It is important to note that the overall magnitude of the JT distortions in isolated B_{12} clusters is rather small, as the bond lengths and bonding angles vary within

$\sim 0.1 \text{ \AA}$ and $\sim 5^\circ$, respectively (Fig. 3.3); DFT calculations show that the energy gain resulting from JT distortions is within 0.2–0.3 eV per B_{12} cluster.

These results suggest that the JT structural lability of the B_{12} units in the crystal lattice of metal dodecaborides RB_{12} may play an important role in the microscopic mechanism of lattice distortions of RB_{12} at low temperature. It should be borne in mind, however, that in the actual crystal structure of RB_{12} , the B_{12} clusters are connected by B-B covalent bonds to form an extended 3D covalent boron network, in which HOMOs of individual B_{12} clusters may have non-integer electron occupation. Nevertheless, one can expect that in RB_{12} crystals some fraction of the JT activity of B_{12} clusters may retain in the three-dimensional boron network because the local triply degenerate HOMOs of B_{12} cuboctahedra remain partially filled, as can be seen from the overall electron balance between the metal and boron sublattices. Due to interactions between the nearest B_{12} clusters in a RB_{12} crystal, local JT distortions of B_{12} cuboctahedra become mutually consistent resulting in a symmetry-lowering distortion of the lattice; this phenomenon is known as the cooperative JT effect, which is well documented in the literature [30–32].

In a concentrated JT system, the full JT Hamiltonian of the crystal is given by the equation [31,32]:

$$\hat{H} = \sum_{\mathbf{n}} \hat{H}_{\text{JT}}(\mathbf{n}) + \frac{1}{2} \sum_{\substack{\mathbf{n}, \mathbf{m} \\ (\mathbf{n} \neq \mathbf{m})}} \mathbf{Q}^+(\mathbf{n}) \hat{K}(\mathbf{n} - \mathbf{m}) \mathbf{Q}(\mathbf{m}), \quad (3.1)$$

where the vector indices \mathbf{n} and \mathbf{m} enumerate unit cells of the crystal, $\hat{H}_{\text{JT}}(\mathbf{n})$ is the one-center JT Hamiltonian for unit cell \mathbf{n} , and the last term represents pairwise interactions between the local JT centers \mathbf{n} and \mathbf{m} . Here $\mathbf{Q}(\mathbf{n})$ is a vector whose components are the local JT-active vibrational modes and $\hat{K}(\mathbf{n} - \mathbf{m})$ is the operator describing interactions between the local JT vibrational modes on sites \mathbf{n} and \mathbf{m} . The electronic and geometric structure of a cooperative JT system is determined from the minimization of the total energy of the crystal resulting from the competition of the local distortions, the first term in Eq. (3.1), and the interaction between the different sites (the second term). In the general case,

10 | Chapter 3 Crystal structures of dodecaborides: complexity in simplicity

cooperative JT interactions can lead to a variety of situations, depending on the specific character of orbitally-degenerate moieties and interplay between the on-site and inter-site JT interactions. In particular, lower symmetry structures in RB_{12} resulting from these cooperative interactions can lead to a parallel alignment of all the local distortions of B_{12} cubooctahedra (which is termed as *ferrodistortive* case) or to a more complicated geometrical arrangement of the local B_{12} distortions (so-called *antiferrodistortive* case). In the ferrodistortive phase, the local JT centers are coupled to a strain of the lattice, which changes the shape of the crystal and its unit cell parameters; this strain mode coupling provides an effective long-range interaction between the JT centers.

It is important to note that in most cooperative JT systems the coupling is predominantly to a strain of the lattice [31, 32]. This fact gives an idea of the origin of observed anomalous behavior of RB_{12} dodecaborides: in fact, formation of a ferrodistortive JT phase with a long-range ordering of JT distortions mediated by the strain of the lattice is the most likely scenario in metal dodecaborides.

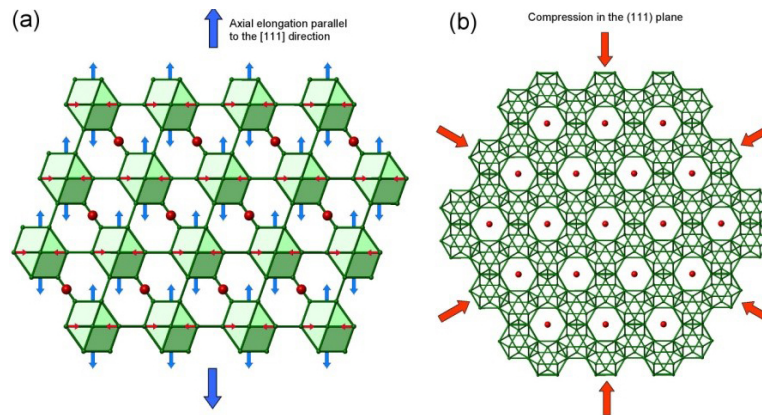


Figure 3.4 Structure of the ferrodistortive JT phase in RB_{12} dodecaborides and the character of the strain of the crystal lattice. (a) The B_{12} cubooctahedra are all elongated along the trigonal axis $[111]$ and compressed in the orthogonal plane; this geometry corresponds to one of the local trigonal JT minima of B_{12} shown in Fig. 3.3; (b) The crystal lattice of RB_{12} is compressed in the (111) plane.

More specifically, the ferrodistoritive JT phase of RB_{12} with the elastic strain axis parallel to the $[111]$ direction seems to be the actual situation that may account for the unusual behavior of RB_{12} . In this case, when the strain mode corresponds to elongation, the B_{12} cuboctahedra are all elongated along the trigonal axis $[111]$, that refers to one of the trigonal JT minima shown in Fig. 3.3; the local distortion JT axes are all parallel to each other [Fig. 3.4 (a)]. Since the elastic strain does not change the volume of the crystal, elongation in the $[111]$ directions is followed by compression in the (111) plane, as depicted in Fig. 3.4 (b).

This leads to important changes in the electronic band structure caused by the trigonal strain mode, as the compression in the (111) plane gives rise to some shortening in the R - R distance between the neighboring metal atoms [Fig. 3.5 (a,b)]. This would change orbital interactions between the R and B atoms responsible for the formation of the electronic conduction band of RB_{12} , which is mainly represented by $2p(B)$ and $5d(R)$ atomic orbitals. The largest changes are expected for the $5d_{z^2}$ metal orbitals that have the strongest σ -type overlap with the $2p$ valence orbitals of boron [Fig. 3.5 (c)]. Accordingly, enhanced $5d_{z^2}(R)$ - $2p(B)$ orbital overlap increases the energy dispersion of the electronic conduction band, thereby increasing the overall number of the filled conduction band state below the Fermi level of RB_{12} . This results in larger electron population of the $5d_{z^2}(R)$ orbitals oriented along the local R - R lines connecting neighboring R atoms in the (111) plane [Fig. 3.5 (c)]. Considering the elongated shape of $5d_{z^2}(R)$ orbitals, this leads to increased electron density along the R - R lines being parallel to the side diagonals $[110]$, $[0\bar{1}1]$, $[101]$, which are shown with red solid lines in Fig. 3.6. These findings are in excellent agreement with the recent experimental results on LuB_{12} , which reveal lower-symmetry electron density distribution (charge stripes) correlating with the filamentary structure of conduction channels observed in the magnetoresistance measurements [33]. Remarkably, the general character of the residual density distribution near the metal atom in the (100) and (010) planes at low temperatures (50 K) shown in Fig. 3.15 strongly resembles the shape of $5d_{z^2}(R)$ orbitals oriented along the R - R lines, as depicted in Fig. 3.5 and Fig. 3.6.

12 | Chapter 3 Crystal structures of dodecaborides: complexity in simplicity

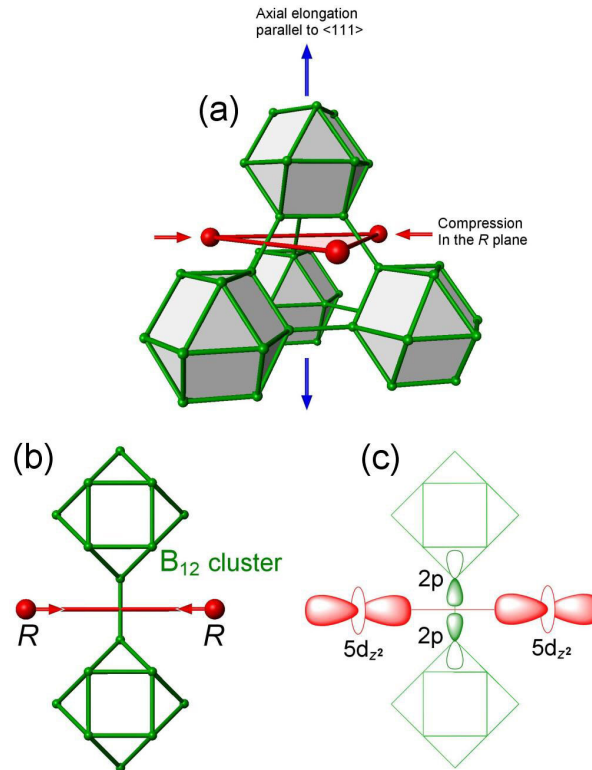


Figure 3.5 On the origin of charge stripes in the ferrodistortive JT phase in RB_{12} dodecaborides, (a) The general character of the local distortions in the ferrodistortive JT phase, (b) reduction of the R - R distance between the neighboring metal atoms due to compression in the (111) plane, (c) orientation of $5d_{z^2}$ metal orbitals having the strongest σ -type overlap with the $2p$ valence orbitals of boron; shortening of the R - R distance leads to a maximal change in the $5d_{z^2}(R)$ - $2p(B)$ orbital overlap, which ultimately causes transfer of excess electron density to the $5d_{z^2}$ orbitals and formation of the charge stripes (see Figs. 3.15 and 3.16 later in the text).

Thus, a theoretical model based on the cooperative JT effect provides a new insight into the microscopic origin of the mysterious structural behavior of RB_{12} cubic dodecaborides. The main reason behind the manifestation of low-symmetry effects of RB_{12} lies in the inherent structural lability of the B_{12} cuboctahedral units

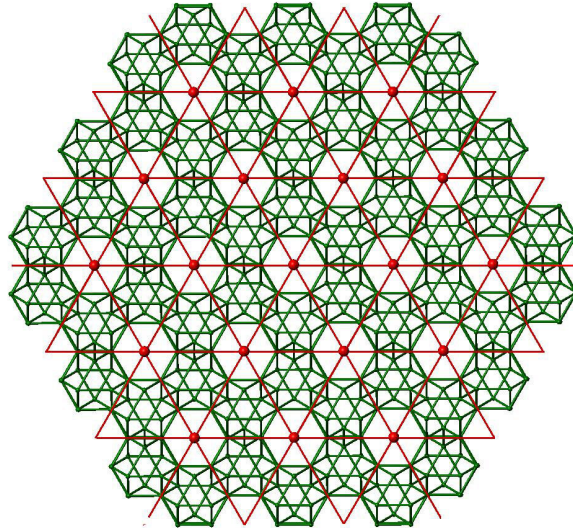


Figure 3.6 Orientation of the charge stripes (the solid red lines) in the (111) plane of RB_{12} resulting from the electron density transfer to the $5d_{z^2}(R)$ orbitals caused by the elastic strain of the crystal lattice in the ferrodistoritive JT phase (see Fig. 3.5).

resulting from their orbital degeneracy and the JT effect. Assuming a ferrodistoritive JT ordering in RB_{12} with deeper trigonal JT minimum of B_{12} clusters enables one to rationalize in a natural way the main experimental results on dodecaborides (see following sections of this chapter for more details):

- (1) The cooperative JT model explains the presence of small distortions of the cubic lattice of RB_{12} at all temperatures, including room temperature. Indeed, in the ferrodistoritive JT state distortions persist at all temperatures, without a structural phase transition. Theoretical treatment of the ferrodistoritive JT state is similar to that for a magnetic spin lattice in an external magnetic field, which always retains some magnetization [31,32]; the latter serves as an order parameter, whose analog in RB_{12} dodecaborides corresponds to the relative magnitude of the deviation from the regular cubic structure.

14 | Chapter 3 Crystal structures of dodecaborides: complexity in simplicity

- (2) The JT model provides a physically transparent insight into the origin of lower symmetry electron density distribution in RB_{12} , including appearance of charge stripes in LuB_{12} and the filamentary structure of conduction channels resulting in anisotropic magnetoresistance [33]. These effects are mainly due to enhanced electron occupation of the $5d_{z^2}$ metal orbitals resulting from the larger $5d(R)-2p(B)$ orbital overlap caused by elastic shortening in the (111) plane in the ferrodistorptive JT state (Figs. 3.4 and 3.5).
- (3) The above consideration indicates that low-symmetry distortions are a unique property of all rare-earth dodecaborides, as they result from the JT structural lability of B_{12} units, not from the ground-state characteristics of the metal ions R .
- (4) This theoretical approach evidently demonstrates that subtle structural departures from the regular cubic structure of RB_{12} dodecaborides are by no means an artifact of x-ray diffraction analysis, but they are an inherent property of all rare-earth RB_{12} compounds resulting from the JT activity of the B_{12} units. Indeed, in the ferrodistorptive JT state, arbitrarily weak JT interactions always lead to a static lattice distortion, by analogy with the nonzero magnetization of the spin system in an external magnetic field. More specifically, this property originates from the fact that the energy gain resulting from the JT distortions grows linearly with the strain value e , while the competing elastic energy is proportional to e^2 ; therefore, at small strains the low-symmetry JT state lies lower in energy [30–32].
- (5) In fact, the presence of significant $^{10}B/^{11}B$ isotope effects in itself suggests the JT origin of the structural instability, since it documents a breakdown of the Born-Oppenheimer approximation for the orbitally degenerate systems, in which electronic and vibrational motions are no longer independent. Generally, isotope effects are more pronounced for the dynamic JT effect, when the JT stabilization energy competes with the vibrational energy; this situation is likely to occur in RB_{12} .

3.3 Modeling the dynamics of the dodecaboride lattice using x-ray diffraction data

Experimental conditions, such as the sample temperature, can vary to better identify the barely perceptible symmetry violations, which may appear due to the cooperative JT effect. The most known phenomenon is the temperature dependence of the unit-cell values, which should be monotonous in the absence of a lattice transformation (see below). Additional information can be obtained by analyzing atomic displacement parameters (ADPs) at different temperatures using both experimental and theoretical temperature curves.

The key role in the structure analysis of crystals is assigned to structure factors $F(\mathbf{H})$, which provide a transition from measured intensities of diffraction peaks to the distribution of electron density in the crystal. The expression for $F(\mathbf{H})$ is as follows:

$$F(\mathbf{H}) = \sum_{\nu=1}^N f_{\nu}(|\mathbf{H}|) \exp(2\pi i \mathbf{r}_{\nu} \cdot \mathbf{H}) T_{\nu}(\mathbf{H}). \quad (3.2)$$

Here $\mathbf{H} = h\mathbf{a}^* + k\mathbf{b}^* + l\mathbf{c}^*$ is a scattering vector; $f_{\nu}(|\mathbf{H}|)$ is the atomic scattering factor of the atom at \mathbf{r}_{ν} ; $T_{\nu}(\mathbf{H}) = \int p(\mathbf{u}_{\nu}) \exp(2\pi i \mathbf{u}_{\nu} \cdot \mathbf{H}) d^3\mathbf{u}$ is the temperature factor, which is known also as the Debye-Waller factor that accounts for the atomic displacements \mathbf{u}_{ν} from the lattice points. Summation is carried out over all atoms in the unit cell of the crystal. As one can see, the temperature factor $T_{\nu}(\mathbf{H})$ is the Fourier transform of the probability density function $p(\mathbf{u}_{\nu})$ whose coefficients are atomic displacement parameters (ADPs) discussed below. The $p(\mathbf{u}_{\nu})$ function can be approximated respectively by univariate or trivariate Gaussian in case of isotropic or anisotropic harmonic vibrations of an atom, and it can be more complicated in case of anharmonic vibrations as a result of heating, for instance. In any case, however, the temperature does not participate directly in the calculations either as a fixed parameter or as a refined variable. Moreover, the conventional approach does not require any assumption of the atomic displacement nature. The ADP values may correspond to thermal vibrations supplemented with static shifts [34]. Along with the atomic coordinates, ADPs are the refined parameters of the struc-

tural model. The least-squares refinement procedure consists in approximation of $|F_{\text{calc}}(\mathbf{H})|^2$ calculated by the formula (3.2) with $|F_{\text{obs}}(\mathbf{H})|^2$, whose values are proportional to the measured intensities of the diffraction reflections. The displacements of each atom are represented in the structural model by one or more parameters, depending on the chosen formalism (isotropic, anisotropic harmonic or anharmonic displacements). Harmonic ADPs form a second-rank matrix $\{u_{ij}\}$, $1 \leq i, j \leq 3$, the trace of which gives an estimate of the equivalent atomic displacements $\langle u^2 \rangle_{\text{eq}}$ or u_{eq} in short notation, $u_{\text{eq}} = (u_{11} + u_{22} + u_{33})/3$. This parameter often appears in studies of the thermal properties of solids.

An alternative method of quantifying atomic displacement parameters is not tied directly to a structural model. Thermal vibration amplitudes $u_{\text{calc}}(R)$ of the metal atoms in the large cavities of the dodecaboride structure well correspond to the Einstein model [35] for independent harmonic oscillators supplemented with a temperature independent static component $\langle u^2 \rangle_{\text{shift}}$ or u_{shift} in short notation:

$$u_{\text{calc}}(R) = \frac{\hbar^2}{k_{\text{B}}m_{\text{a}}T_{\text{E}}} \left(\frac{1}{2} + \frac{1}{\exp(T_{\text{E}}/T - 1)} \right) + u_{\text{shift}}(R) \quad (3.3)$$

The expanded Debye model [36] is suitable for atoms of the boron framework whose displacements strongly correlate with each other:

$$u_{\text{calc}}(\text{B}) = \frac{3\hbar^2}{k_{\text{B}}m_{\text{a}}T_{\text{D}}} \left(\frac{1}{4} + \left(\frac{T}{T_{\text{D}}} \right)^2 \int_0^{\frac{T_{\text{D}}}{T}} \frac{y \, dy}{\exp(y) - 1} \right) + u_{\text{shift}}(\text{B}) \quad (3.4)$$

The agreed notations are: $\hbar = h/2\pi$ is the Planck constant; k_{B} — the Boltzmann constant; m_{a} — atomic mass; T_{E} (T_{D}) — the characteristic Einstein (Debye) temperature; T — the temperature of the experiment.

The problem is that the characteristic Einstein (Debye) temperature and the value of u_{shift} must be known in advance to calculate the values of u_{calc} from Eqs. (3.3) or (3.4). Still, it is possible to solve the inverse problem of calculating the characteristic Einstein (Debye) temperature and u_{shift} using the values of u_{eq} determined from diffraction data. For this purpose, one should collect the multi-temperature data sets $\{h, k, l, |F_{\text{obs}}|, \sigma_F\}$ and refine the crystal structure at each temperature using conventional

3.3 Modeling the dynamics of the dodecaboride lattice using x-ray diffraction data | 17

techniques. As a result, each atom is supplied at each temperature with a value of $u_{\text{obs}} = u_{\text{eq}}$. The multi-temperature set of these parameters then serves as an input for a least-squares procedure $\sum |u_{\text{calc}}^2 - u_{\text{obs}}^2| \rightarrow \min$ to fit the model curve to the set of u_{obs} . The characteristic Einstein (Debye) temperature T_D (T_E) and the value of u_{shift} are adjustable parameters of this procedure [37].

Thus, the proposed approach [37] allows us to solve several problems at once:

- (1) to obtain the Einstein (Debye) characteristic temperatures estimated otherwise from the heat capacity or somehow else;
- (2) to describe the temperature dependence of the thermal atomic vibrations using an appropriate analytical function;

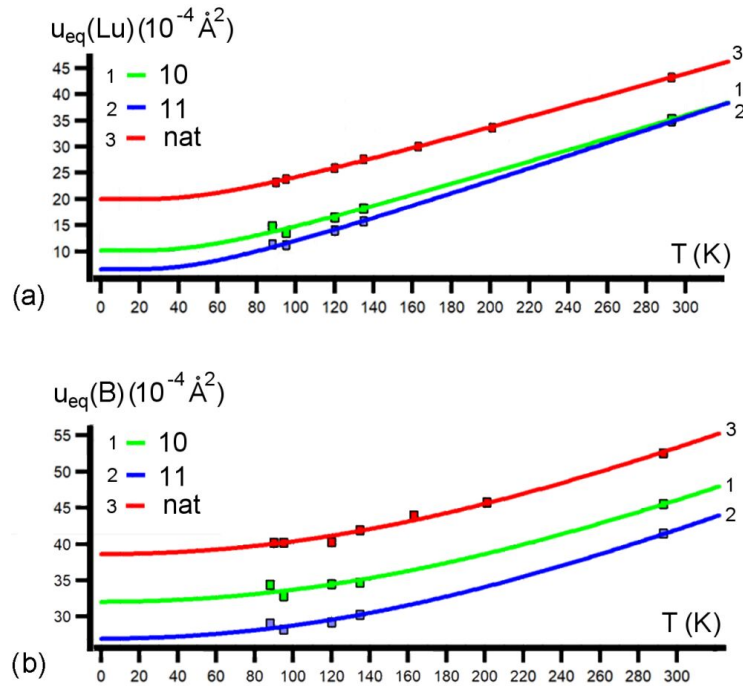


Figure 3.7 Temperature dependencies of u_{eq} in the crystals of Lu^NB_{12} ($N = 10, 11, \text{nat}$). The Einstein (a) and Debye (b) models are used respectively for Lu and B atoms. The fit is based on the u_{obs} values marked with squares [38].

18 | Chapter 3 Crystal structures of dodecaborides: complexity in simplicity

- (3) to separate the contributions of the static and dynamic components into the equivalent parameter u_{eq} of atomic displacements.

The Debye and Einstein models were previously used to fit the multi-temperature ADPs and to estimate the Debye (Einstein) temperatures in crystals of various compositions including hexaborides RB_6 ($R = \text{Y, La-Gd}$) [39–42]. This approach, being first applied to the dodecaborides Lu^NB_{12} ($N = 10, 11, \text{nat}$), revealed a difference in the static components u_{shift} depending on the isotope composition of boron [38]. The abbreviation 'nat' is hereinafter used to refer to natural boron with the ratio $^{10}\text{B}:^{11}\text{B} \approx 19.8:80.2$. Refined values of T_E (T_D) and u_{shift} were substituted in the Eqs. (3.3) and (3.4) to draw the curves for Lu and B presented in Figs. 3.7 (a) and (b), respectively.

The ADPs sum up mean-square zero vibrations $\langle u^2 \rangle_{\text{zero}}$, temperature-dependent thermal vibrations $\langle u^2(T) \rangle$, and static

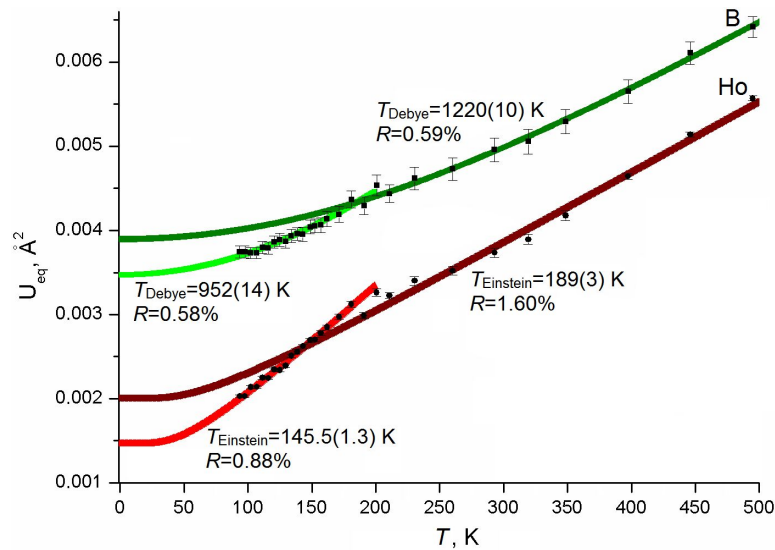


Figure 3.8 Experimental ADPs (u_{eq}) in HoB_{12} are fitted using the Einstein (for Ho) and Debye (for B) models in temperature ranges 86–180 and 210–500 K. $R = \sum |u_{\text{obs}}^2 - u_{\text{calc}}^2| / \sum u_{\text{obs}}^2$.

3.4 Modeling the dynamics of the dodecaboride lattice using x-ray diffraction data | 19

shifts $\langle u^2 \rangle_{\text{shift}}$. The curves in Fig. 3.7 are plotted for three crystals with very close Debye (Einstein) temperatures, so that $u_{\text{eq}}(T)$ mostly differ in their temperature independent components $\langle u^2 \rangle_c = \langle u^2 \rangle_{\text{zero}} + \langle u^2 \rangle_{\text{shift}}$. As shown in [38], these components are maximal in $\text{Lu}^{\text{nat}}\text{B}_{12}$ both for Lu and B atoms. Static distortions of boron polyhedra are combined with static shifts of Lu atoms from the lattice points, which can be explained by disorder in ^{10}B - ^{11}B substitution in the crystal with natural boron.

The structure of single-crystal HoB_{12} was studied by x-ray diffraction analysis in the $Fm\bar{3}m$ group at 29 temperatures in the range of 86–500 K [43]. Temperature variations of $u_{\text{eq}}(\text{B})$ and $u_{\text{eq}}(\text{Ho})$ lose stability near 200 K. To improve the fit, one has to divide each of the experimental sets of u_{eq} into two parts obtained in the 86–180 K and 210–500 K temperature ranges, and to build two curves for each atom (Fig. 3.8) for better modeling of the experimental curves. The instability of the unit-cell values could be clearly determined from the x-ray data not only in HoB_{12} in the temperature range 150–200 K, but also in $R\text{B}_{12}$ ($R = \text{Ho}, \text{Tm}, \text{Yb}, \text{Lu}$) below 200 K (see Figs. 3.9–3.13 in the next section). The development of similar lattice instability with decreasing temperature was also reported earlier in Lu^NB_{12} crystals with different isotopic boron composition ($N = 10, 11, \text{nat}$) that were studied using low-temperature heat capacity and Raman scattering data [24]. The maximum density of vibrational states was observed at the temperature near 150 K [24]. It was noted that the mean free path of phonons reaches the Ioffe-Regel limit in the vicinity of this temperature, being compared with their wavelength. Remarkable spectral changes in the zero-field spectra and a sharp maximum in the relaxation rate were recorded near 150 K in μSR experiments for dodecaborides $R\text{B}_{12}$ ($R = \text{Yb}, \text{Lu}$) and solid solutions $\text{Lu}_{1-x}\text{Yb}_x\text{B}_{12}$. It has been suggested that the large-amplitude dynamic features arise from atomic motions within the B_{12} clusters [44, 45]. Most likely, the instability of u_{eq} is caused by changes in the phonon structure of the rare-earth dodecaborides and is not a unique feature of only HoB_{12} .

3.4 Crystal structure: problems and results

3.4.1 *The Jahn-Teller distortions of structural parameters*

Active studies of the RB_{12} structure at various temperatures, which were started in the early 2000s but not continued at that time, were resumed later after the tetragonal distortion of the LuB_{12} structure had been confirmed in the temperature range 50–75 K [48]. The structure of a LuB_{12} single crystal was then thoroughly studied at room temperature [49]. The single crystals of LuB_{12} were grown by modified crucibleless inductive floating zone melting using high-purity source materials: lutetium oxide Lu_2O_3 and boron [17]. One of the purposes of the re-examination of the known structure was to assess the suitability of the grown single crystals for accurate structure analysis. The refinement of the structural model in the $Fm\bar{3}m$ symmetry group with a uniquely low residual factor $R = 0.2\%$ was made possible due to the high diffraction quality of the single crystals combined with a set of original experimental techniques [50–52] that ensured the accuracy and reliability of the x-ray data measured.

Besides that, accurate measurements of the periods of the LuB_{12} crystal lattice were carried out in the temperature range 20–295 K [53]. Two periods $a \approx b$ did not differ within the limits of the standard uncertainty (σ), but the third period c steadily deviated downward by 2σ or more over practically the entire temperature range. In absolute values, the difference in the lattice constants is very small (about 0.002 \AA), which is an order of magnitude less than in the lattice of ScB_{12} . Such a small difference in the lattice constants does not give grounds for a revision of the structural model, especially in view of what was said above about the excellent results of the refinement of the cubic structure of LuB_{12} . However, even very small differences in the lattice constants can have a significant effect on the physical properties of crystals. The lattice parameters must be determined for many dodecaborides of different composition in a wide temperature range without symmetry restrictions in order to collect experimental information on the Jahn-Teller distortions. This work is still far from complete, both in the number of crystals studied and in the number of tem-

3.4 Crystal structure: problems and results | 21

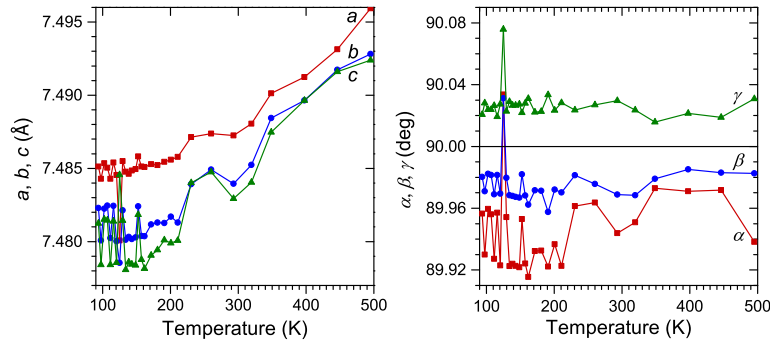


Figure 3.9 Linear (a, b, c) and angular (α, β, γ) unit-cell parameters of HoB_{12} in the temperature range 85–500 K [43].

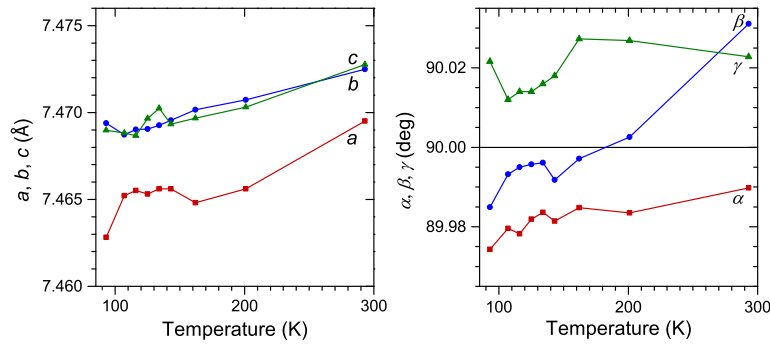


Figure 3.10 Linear (a, b, c) and angular (α, β, γ) unit-cell parameters of TmB_{12} in the temperature range 85–300 K [46].

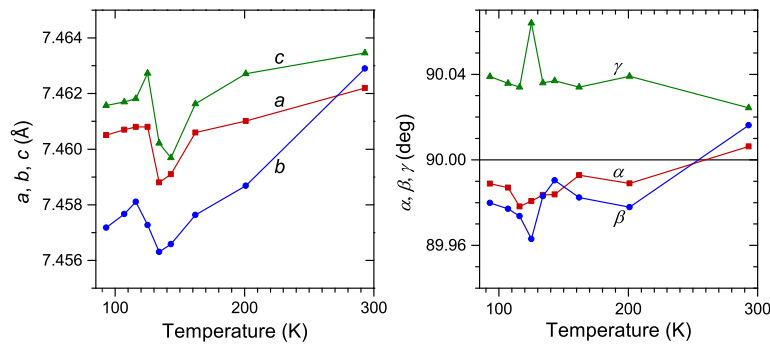


Figure 3.11 Linear (a, b, c) and angular (α, β, γ) unit-cell parameters of YbB_{12} in the temperature range 85–300 K [47].

22 | Chapter 3 Crystal structures of dodecaborides: complexity in simplicity

perature points measured. After the first experiments with LuB_{12} , linear and angular unit-cell parameters have been determined at various temperatures for HoB_{12} , TmB_{12} , and YbB_{12} as shown in Figs. 3.9–3.11.

The linear parameters always manifest small tetragonal-type distortions. Note that one lattice constant of LuB_{12} and TmB_{12} is smaller than the other two: $a \approx b > c$ (the unit cell is slightly compressed along an edge), whereas one lattice constant of HoB_{12} is slightly elongated: $a > b \approx c$. Both linear and angular parameters of each unit cell undergo the most noticeable non-linear changes in the same low-temperature region between 100 and 150 K. It is noteworthy that lattices of TmB_{12} and YbB_{12} undergo opposite changes despite the proximity of Tm and Yb in the series of rare earth elements. Closer to the middle of the mentioned temperature range, the lattice constants of YbB_{12} abruptly decrease and return to the former, even slightly larger values with a further decrease in temperature. The obliquity of the YbB_{12} lattice slightly increases, but then the angles return to their previous values. At the same temperatures, the periods of the TmB_{12} lattice slightly increase, and the angles become slightly closer to 90° .

3.4.2 Structural peculiarities of dodecaborides different in isotopic boron composition

Since the cooperative JT effect is determined by the dynamics of light boron atoms, one can suppose that isotope substitutions ^{10}B - ^{11}B may affect both properties and crystal structure of dodecaborides. Till recently, the research was mainly limited to physical properties [9, 17, 24–26]. Thermal expansion of $\text{Lu}^{10}\text{B}_{12}$ and $\text{Lu}^{\text{nat}}\text{B}_{12}$ was studied based on the x-ray powder diffraction data in the temperature range 10–290 K [54]. Both samples showed negative thermal expansion between 50 and 100 K (Fig. 3.12).

This is consistent with the temperature region in which the negative thermal expansion was previously observed for $\text{Lu}^{\text{nat}}\text{B}_{12}$ by the three-terminal capacitive method [15]. The lattice constant of $\text{Lu}^{10}\text{B}_{12}$ is increased relative to that of $\text{Lu}^{\text{nat}}\text{B}_{12}$ by 0.001–0.002 Å over the measured temperature range. The β -rhombohedral boron lattices have the same property, but the difference between the

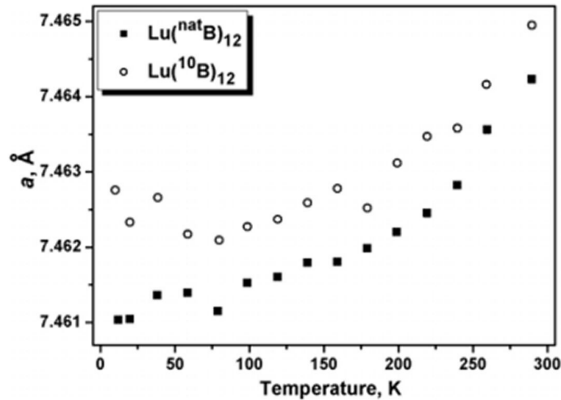


Figure 3.12 The lattice parameter vs. temperature in LuB_{12} containing natural boron and ^{10}B isotope [8].

lattice parameters in the crystals with 10% and 97% content of ^{10}B is more noticeable (about 0.03 Å) as established in Ref. [55] whose authors presented a theoretical justification for such an expansion of the ^{10}B lattice.

An influence of the isotopic composition on the structure and properties of Lu^NB_{12} , $N = 10, 11, \text{nat}$, was studied in [38]. Taking into account both linear and angular distortions of the unit cells of the three crystals, one can conclude that the $\text{Lu}^{10}\text{B}_{12}$ lattice is distorted rather by tetragonal type $a \approx b > c$ whereas the distortions of the $\text{Lu}^{11}\text{B}_{12}$ lattice are more similar to pseudo-trigonal ones $a \approx b \approx c$, $\alpha \approx \beta \approx \gamma > 90^\circ$. Lattice distortions of $\text{Lu}^{\text{nat}}\text{B}_{12}$ have an intermediate character (see Fig. 3.13).

At temperatures below 140 K, the distortions are nonlinear, as can be assumed despite the small number of the points measured. Nonlinear distortions of the parameters, which occur at close temperatures in three different crystals, are hardly explained by a sheer accident. At a temperature of about 120 K, the trigonal-type distortions of the lattices of $\text{Lu}^{11}\text{B}_{12}$ and $\text{Lu}^{\text{nat}}\text{B}_{12}$ are amplified, as well as the pseudo-tetragonal lattice distortions of $\text{Lu}^{10}\text{B}_{12}$ crystal, but the situation changes again with a further decrease in temperature. Thus, we observe the same jump in the parameters of the unit cell

24 | Chapter 3 Crystal structures of dodecaborides: complexity in simplicity

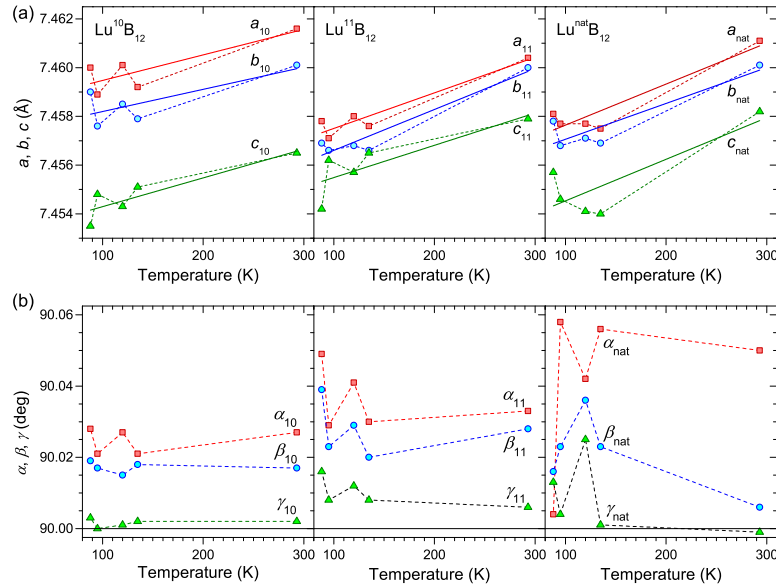


Figure 3.13 Temperature dependences of the lattice parameters for Lu^NB_{12} over the temperature range 88–293 K: (a) lattice constants; (b) unit-cell angles. Experimental values are connected by dashed lines; solid lines in panel (a) are linear fits. Standard uncertainties do not exceed 0.0002 Å and 0.001° , respectively [38].

approximately in the middle of the temperature range 100–150 K as in other three dodecaborides mentioned above. It is worth noting that 120 K is close to the upper boundary of the temperature interval with negative thermal expansion of $\text{Lu}^{\text{nat}}\text{B}_{12}$ according to Refs. [14, 15].

3.4.3 Formation of charge stripes in voids of the crystal lattice

The numerical differences between the lattice parameters are very small and do not require a transition to the low-symmetry structure model. The crystal structures of LuB_{12} , TmB_{12} , HoB_{12} and many other dodecaborides can be successfully refined in the cubic group $Fm\bar{3}m$ with low values of R -factors. It should be noted, however,

that the completeness of the structural analysis is judged not only by the R -factor value but also by the distribution of the residual electron density (ED) on the difference Fourier maps. Fourier synthesis of the electron density is a computational procedure, which starts with a set of both experimental and previously calculated parameters. The computational formula can be written in general terms as follows:

$$G(\mathbf{r}) = \frac{1}{V} \sum_{\mathbf{H}} A(\mathbf{H}) \exp[i\varphi(\mathbf{H})] \exp(-2\pi i \mathbf{H} \cdot \mathbf{r}). \quad (3.5)$$

Here $G(\mathbf{r})$ is either full (g) or residual (Δg) electron density, resulting respectively either from a “regular” or difference Fourier synthesis; V is the unit-cell volume; $\mathbf{H} = \sum_i h_i \mathbf{a}_i^*$ is a scattering vector; and $\varphi(H)$ is a scattering phase. $A(\mathbf{H})$ are coefficients dependent on the type of the Fourier synthesis. In case of difference Fourier synthesis, $A(\mathbf{H}) = ||F_{\text{obs}}(\mathbf{H})| - |F_{\text{calc}}(\mathbf{H})||$ is a difference between observed and calculated absolute values of the structure factor. The first value is the square root of the reflection intensity whereas the second one is calculated from atomic coordinates and ADPs, whose values are refined using a least-square technique.

As follows from Eq. (3.5), the Fourier synthesis of the electron density does not require any data on the crystal symmetry. It can be performed independently in each point of the crystal lattice. Nevertheless, the symmetry of the crystal is usually taken into consideration in the algorithms that implement Fourier synthesis of the electron density. It means that the measured intensities of x-ray reflections are averaged in the corresponding Laue class and the Fourier synthesis is performed in a symmetrically independent region of the unit cell. As a result, the symmetry of the Fourier map exactly corresponds to the space group, information about which is fed to the input of the computational procedure. Certainly, any measurement is not free from the influence of instrumental errors and the data processing methods. On the one hand, the above-mentioned techniques of calculations are designed to improve the accuracy of the results and to ensure visual consistency of the Fourier maps with the stated symmetry of the crystals. On the other hand, averaging can harm since the symmetry of the electron-density distribution over the cell can be overestimated.

26 | Chapter 3 Crystal structures of dodecaborides: complexity in simplicity

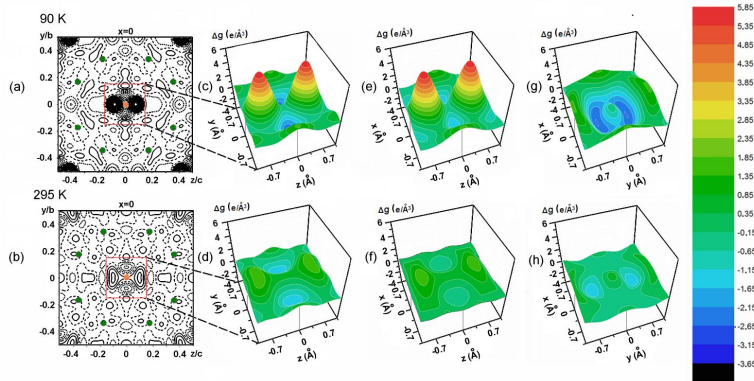


Figure 3.14 Difference Fourier maps (residual electron density Δg in $e/\text{\AA}^3$) in the $x = 0$ face of the LuB_{12} unit cell at (a) 90 K and (b) 295 K. Red circle is the Lu site; green circles are B sites. The panels (c)–(g) and (d)–(e) are the surface plots of difference Fourier maps in the vicinity of the Lu ion, in the $x = 0$, $y = 0$, and $z = 0$ faces of the unit cell, respectively. The first and second rows of the figure correspond to temperatures 90 K and 295 K, respectively [27].

In the case when accuracy and reliability of measured x-ray data are ensured by reliable measurement of literally each reflection, with subsequent consideration of experimental corrections using special techniques [50–52], one may feed a less symmetrical group to the input of the Fourier procedure. In [27], this approach was applied to LuB_{12} whose structure was first refined in the high-symmetry $Fm\bar{3}m$ group at temperatures 295 and 90 K. After that, the measured values of $|F_{\text{obs}}|$ were averaged in the mmm Laue class instead of $m\bar{3}m$, and the orthorhombic $Fmmm$ group was fed to the input of the difference Fourier procedure, skipping the tetragonal $I4/mmm$ group, which would require a transition to another unit cell. The difference Fourier maps built from low-temperature (90 K) x-ray data clearly showed residual electron-density peaks oriented along $[001]$ at distances of about 0.5 \AA from the central position of Lu. As can be seen from Fig. 3.14, similar peaks are absent along $[010]$, which is symmetrically equivalent to $[001]$ in the cubic group. This result agrees with the result obtained in the same work [27]

3.4 Crystal structure: problems and results | 27

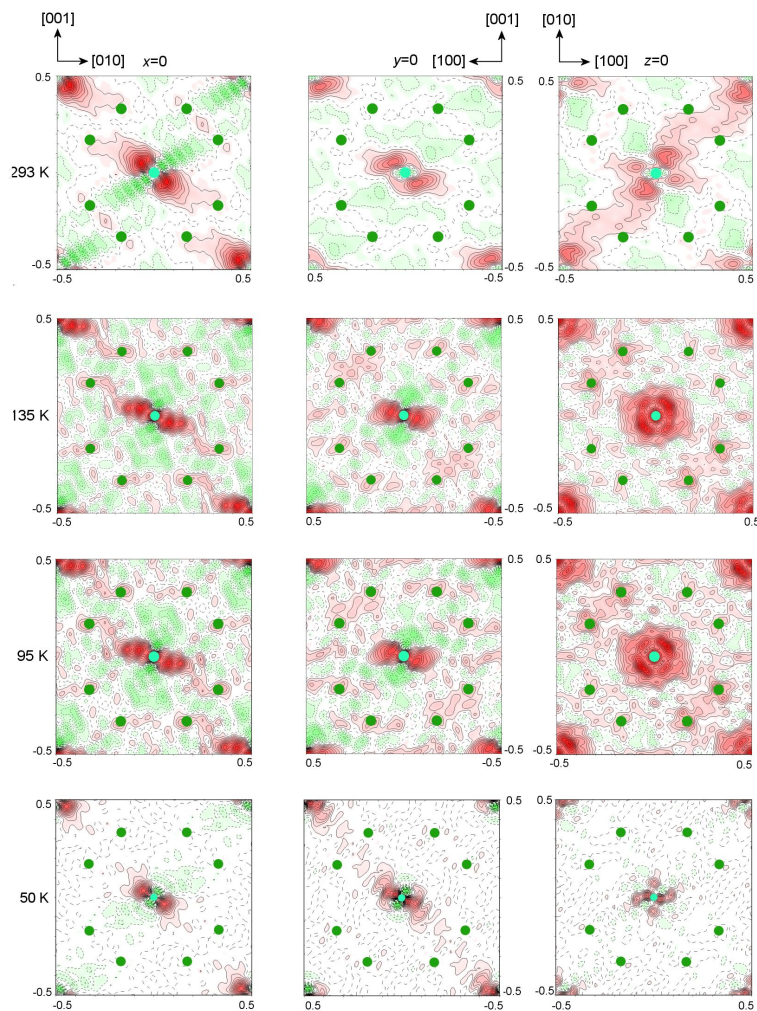


Figure 3.15 Residual electron-density distribution in the $x = 0$, $y = 0$, and $z = 0$ planes of LuB_{12} . Difference Fourier synthesis is done in $F\bar{1}$ using data collected at four temperatures. Contour intervals are $0.2 e/\text{\AA}^3$ (295, 135, 95 K) and $1 e/\text{\AA}^3$ (50 K). Positive (pink) and negative (light-green) residual electron density is highlighted. The central Lu(0,0,0) site (lime green circle) is surrounded by eight boron sites (dark green circles); $[-0.5, 0.5]$ intervals are periods of the crystal lattice [33].

28 | Chapter 3 Crystal structures of dodecaborides: complexity in simplicity

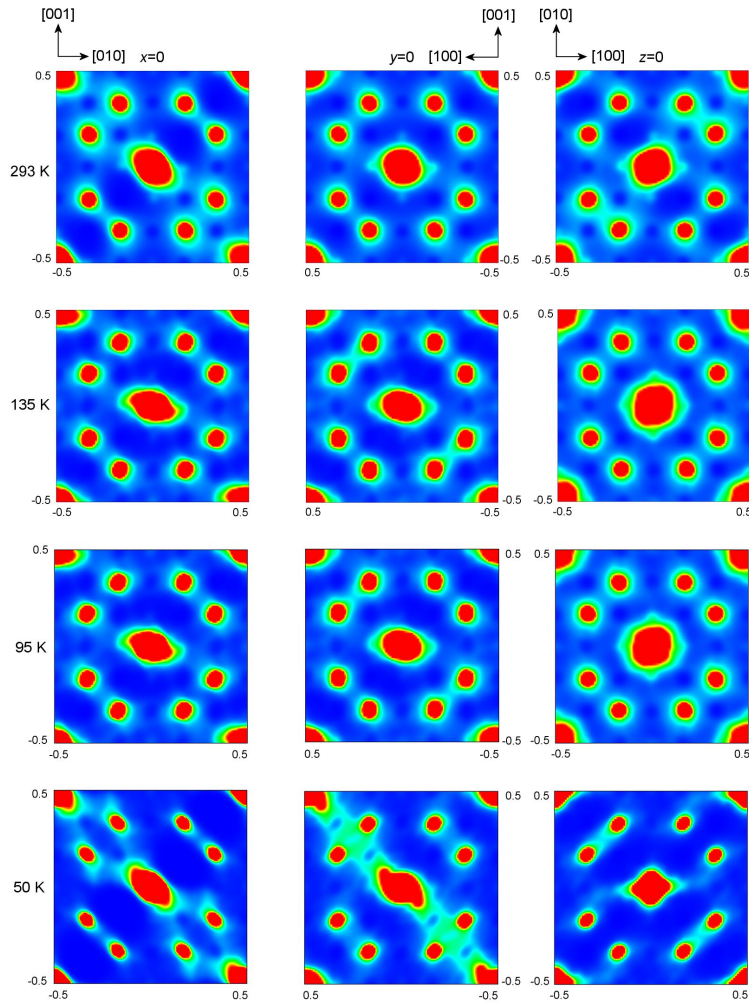


Figure 3.16 Maximum-entropy-method maps are calculated from the LuB_{12} data sets collected at temperatures 293, 135, 95 and 50 K. Three columns from left to right present thin slices of the electron-density distribution in three planes of the crystal lattice. The central Lu is surrounded by eight boron atoms; $[-0.5, 0.5]$ intervals are periods of the crystal lattice [33].

concerning unequal magnetoresistance in the LuB_{12} sample in two directions of the $\langle 100 \rangle$ family.

In the next work [33], the crystal structure of LuB_{12} was studied at the four temperatures 293, 135, 95 and 50 K. To eliminate possible dependence of the results on systematic instrumental errors and on the features of the crystalline sample, the x-ray experiments were performed on three different-type diffractometers and on two LuB_{12} crystals. To analyze the electron-density distribution in the crystal at room temperature, the same data were used that were previously collected on a CAD4 diffractometer (Enraf Nonius) for a precise analysis of the cubic structure of LuB_{12} [49]. The x-ray data at 135 and 95 K were collected on an Xcalibur EOS S2 diffractometer with a two-dimensional CCD detector. The experiment at 50 K was obtained on a four-circle Huber-5042 diffractometer equipped with a point detector and a closed-cycle helium cryostat Displex DE-202. The structure was first refined in $Fm\bar{3}m$ as before, but information on triclinic $F\bar{1}$ symmetry was fed to the input of the Fourier procedure. Non-standard abbreviation $F\bar{1}$ instead of $P\bar{1}$ is due to the reluctance to move to another (non-cubic) cell, which would correspond to the standard setting. The difference Fourier maps were built for each temperature in three sections of a crystal with the (100), (010), (001) planes. As seen from Fig. 3.15, the symmetry of the residual electron-density distribution is clearly lower than orthorhombic. The selected directions remain but lose their exact orientation along the canceled axis 2 of the orthorhombic group, turning in the direction closer to the face diagonal of the unit cell. The residual electron density increases almost by an order of magnitude at the temperature of 50 K forming a continuous diagonal strip in the (010) section. The formation of the electron-density strip at 50 K is confirmed by the maximum entropy method (MEM) as shown in Fig. 3.16.

We associate this observation with the formation of a filamentary structure of conductive channels — charge stripes along selected directions in the crystal [33]. In the same paper, two results were compared, which were obtained on LuB_{12} samples cut from one block. The same sample could not be used in all experiments due to different requirements for its size and shape for x-ray experiments and measurements of transport and magnetic properties.

30 | Chapter 3 Crystal structures of dodecaborides: complexity in simplicity

Moreover, the x-ray measurements were carried out at significantly higher temperatures and in the absence of an external magnetic field. The more surprising is the exact orientational coincidence of two pictures in the left and right parts of Fig. 3.17, one of which (left) illustrates the anisotropy of the transverse magnetoresistance in LuB_{12} whereas the second picture demonstrates the anisotropy of the residual electron-density distribution in LuB_{12} at 50 K.

Another structure of a single-crystal $\text{Tm}_{0.19}\text{Yb}_{0.81}\text{B}_{12}$ was analyzed according to the same scheme at room temperature [56]. Extreme members TmB_{12} and YbB_{12} in a series of solid solutions $\text{Tm}_{1-x}\text{Yb}_x\text{B}_{12}$ vary greatly in their properties, despite the proximity of Tm and Yb in the series of rare-earth elements. Unlike metallic TmB_{12} with antiferromagnetic properties, YbB_{12} is a narrow-gap semiconductor known as a Kondo insulator. In order to analyze the loss of metallic properties when thulium is replaced by ytterbium, the information is needed on the corresponding changes in the crystal structure.

It has been determined that the crystal lattice of $\text{Tm}_{0.19}\text{Yb}_{0.81}\text{B}_{12}$ has the same type of distortion as that of LuB_{12} , with $a \approx b > c$ and a small difference of about 0.002 \AA between the smaller lattice constant and the other two. The residual electron density is oriented predominantly along the three face diagonals of the

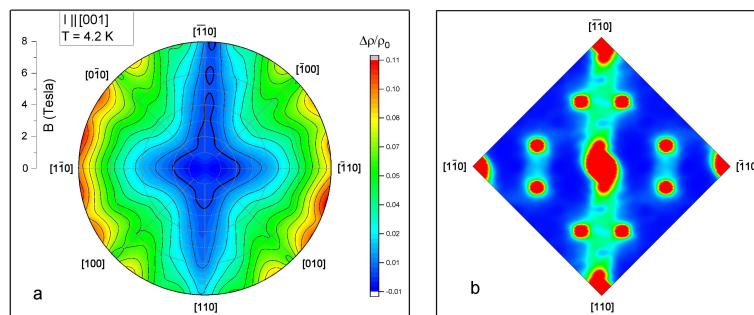


Figure 3.17 (a) Magnetoresistance anisotropy of LuB_{12} in polar coordinates: $\Delta\rho/\rho_0 = [\rho(\varphi, B) - \rho(\varphi_0, B)]/\rho(\varphi_0, B)$, $\varphi_0 = 270^\circ$ corresponding to $\mathbf{B} \parallel [\bar{1}\bar{1}0]$; (b) anisotropic electron-density distribution in a thin layer of the electron density reconstructed by the maximum entropy method [33].

unit cell. They are connected by a spatial diagonal, which is one of the three-fold axes of the undistorted cubic structure. The residual electron density forms a strip along one of the face diagonals even at room temperature, as can be seen in Fig. 3.18.

3.5 Conclusions

The results presented in this chapter demonstrate the complexity of the atomic structure of the dodecaborides, a complete description of which does not fit into the framework of a simple cubic model. Both atomic coordinates being expressed in fractions of the lattice constants and ADPs of almost all dodecaborides correspond well to cubic symmetry and do not require revision of the structural model despite the Jahn-Teller distortion of lattice parameters. Symmetry violations manifest themselves in difference Fourier syntheses as

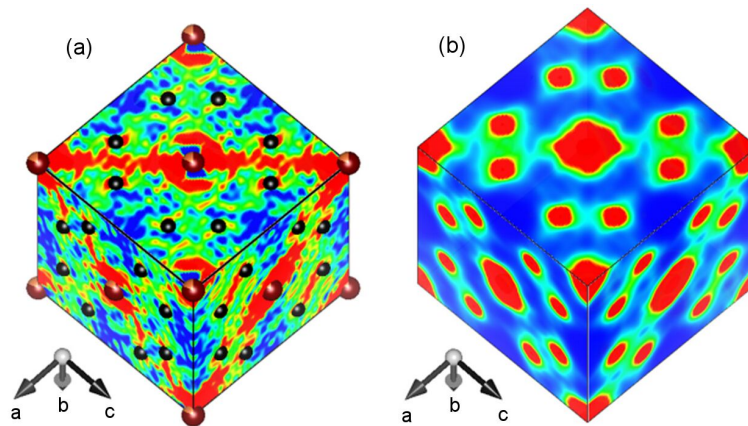


Figure 3.18 (a) Difference Fourier and (b) maximum-entropy-method maps of $\text{Tm}_{0.19}\text{Yb}_{0.81}\text{B}_{12}$ are created in (100), (010), (001) faces of the unit cell. Electron density (g) in the layer of any given thickness is automatically divided into several levels from g_{\min} to g_{\max} , each of them is assigned to a definite color from dark-blue over green to red. The values of g_{MEM} are cut at the level $g_{\max} = 0.075\%$ of the maximal g_{MEM} value to show fine electron-density gradations in the thin layer. Difference electron-density values are cut at $\pm 0.5 e/\text{\AA}^3$ [56].

32 | Chapter 3 Crystal structures of dodecaborides: complexity in simplicity

an asymmetric distribution of the residual electron density in the interstices of the crystal lattice along symmetrically equivalent directions. These results are in good agreement with the observed asymmetry of physical properties (conductive, magnetic).

Another prospective direction of the structural analysis of dodecaborides is the quantitative analysis of the temperature behavior of the atomic displacement parameters using multi-temperature x-ray data. The dynamics of the crystal lattice can be traced without going beyond the cubic structural model, by matching the equivalent atomic displacement parameters to the extended Einstein or Debye models.

The analysis of the dodecaboride structure is thus not limited to the refinement of the structural model in the high-symmetric group at one or several temperatures. The multi-temperature data on ADPs must be supplemented with the temperature dependent unit-cell parameters, which are not bound by the symmetry constraints, and with the difference Fourier maps built without reliance on the symmetry of the structure model.

The transition from single experiments to systematic research of the structure-property relationship in dodecaborides requires the creation of a database of diffraction data. For reliable characterization of a single dodecaboride of a certain composition, it is necessary to carry out a series of diffraction experiments in a wide temperature range with the maximum possible coverage of the low-temperature region. The temperature step should be selected individually for each composition in order to monitor the structural parameters.

Acknowledgments

The authors are grateful to N. E. Sluchanko and N. Yu. Shitsevalova for useful discussions. This work was supported by the Ministry of Science and Higher Education within the state assignment of the Federal Scientific Research Center (FSRC) "Crystallography and Photonics" of the Russian Academy of Sciences in the part related to the development of structural analysis methods. Crystal structures and properties of HoB₁₂ and ErB₁₂ crystals were

studied with the support of the Russian Foundation for Basic Research, Grant No. 18-29-12005; similar studies on TmB_{12} , YbB_{12} , and LuB_{12} were supported by the Russian Science Foundation, grant No. 17-12-01426. The diffraction data were collected using the equipment of the Shared Research Center of the FSRC “Crystallography and Photonics” of the Russian Academy of Sciences and was supported by the Russian Ministry of Education and Science (project RFMEFI62119X0035).

References

- [1] Bertaut, F. and Blum, P.; “La structure des borures d’uranium”; *Comptes Rendus Acad. Sci.* **229**, 666–667 (1949).
- [2] Post, B. and Glaser, F. W.; “Crystal structure of ZrB_{12} ”; *J. Miner. Met. Mater. Soc.* **4**, 631–632 (1952).
- [3] La Placa, S., Binder, I., and Post, B.; “Binary dodecaborides”; *J. Inorg. Nuclear Chem.* **18**, 113–117 (1961).
- [4] Przybylska, M., Reddoch, A. H., and Ritter, G. J.; “The preparation and structure of lutetium diboride, scandium dodecaboride and lutetium antimonide”; *J. Am. Chem. Soc.* **85**, 407–411 (1963).
- [5] Matkovich, V. I., Economy, J., Giese, R. F., and Barrett, R.; “The structure of metallic dodecaborides”; *Acta Crystallogr.* **19**, 1056–1058 (1965).
- [6] Matkovich, V. I. and Economy, J.; “Structural determinants in the higher borides”; in Matkovich, V. I., Samsonov, G. V., Hagenmuller, P., and Lundstrom, T. (eds.), *Boron and refractory borides*, pp. 78–95, (Springer, Berlin, Heidelberg, 1977).
- [7] Flachbart, K., Alekseev, P., Grechnev, G., Shitsevalova, N., Siemensmeyer, K., Sluchanko, N., and Zogal, O.; “Rare-earth dodecaborides — magnetism, superconductivity and other properties”; chap. 2 in Delfrey, K. N. (ed.), *Rare Earths: Research and Applications*, vol. 34, pp. 79–125, (Nova Science Publishers, USA, 2008).
- [8] Mori, T.; “Higher borides”; chap. 238 in Gschneidner Jr., K. A., Bünzli, J.-C. G., Pecharsky, V. K. (eds.), *Handbook on the Physics and Chemistry of Rare Earths*, vol. 38, pp. 105–173, (North-Holland 2008).
- [9] Werheit, H., Filipov, V., Shirai, K., Dekura, H., Shitsevalova, N., Schwarz, U., and Armbrüster, M.; “Raman scattering and isotopic phonon effects in dodecaborides”; *J. Phys.: Condens. Matter* **23**, 065403 (2011).
- [10] Cannon, J. F., Cannon, D. M., and Tracy Hall, H.; “High pressure syntheses of SmB_2 and GdB_{12} ”; *J. Less Common Metals* **56**, 83–90 (1977).

34 | Chapter 3 Crystal structures of dodecaborides: complexity in simplicity

- [11] Akopov, G.; "Rediscovering the crystal chemistry of superhard dodecaborides and other higher borides"; Ph.D. thesis; University of California, Los Angeles (2018).
- [12] Liang, Y., Zhang, Y., Jiang, H., Wu, L., Zhang, W., Heckenberger, K., Hofmann, K., Reitz, A., Stober, F. C., and Albert, B.; "Thermodynamic ground states of multifunctional metal dodecaborides"; *Chem. Mat.* **31**, 1075–1083 (2019).
- [13] Leithe-Jasper, A., Sato, A., and Tanaka, T.; "Refinement of the crystal structure of zirconium dodecaboride, ZrB_{12} , at 140 K and 293 K"; *Z. Kristallogr. NCS* **217**, 319–320 (2002).
- [14] Czopnik, A., Shitsevalova, N., Krivchikov, A., Pluzhnikov, V., Paderno, Y., and Ōnuki, Y.; "Thermal properties of rare earth dodecaborides"; *J. Solid State Chem.* **177**, 507–514 (2004).
- [15] Czopnik, A., Shitsevalova, N., Pluzhnikov, V., Krivchikov, A., Paderno, Y., and Ōnuki, Y.; "Low-temperature thermal properties of yttrium and lutetium dodecaborides"; *J. Phys.: Condens. Matter* **17**, 5971 (2005).
- [16] Menushenkov, A. P., Yaroslavtsev, A. A., Zaluzhnyy, I. A., Kuznetsov, A. V., Chernikov, R. V., Shitsevalova, N. Y., and Filippov, V. B.; "Features of the local structure of rare-earth dodecaborides RB_{12} ($R = Ho, Er, Tm, Yb, Lu$)"; *JETP Lett.* **98**, 165–169 (2013).
- [17] Werheit, H., Paderno, Y., Filippov, V., Paderno, V., Pietraszko, A., Armbrüster, M., and Schwarz, U.; "Peculiarities in the Raman spectra of ZrB_{12} and LuB_{12} single crystals"; *J. Solid State Chem.* **179**, 2761–2767 (2006).
- [18] Pietraszko, A., Czopnik, A., Shitsevalova, N., Paderno, Y., and Pluzhnikov, V.; "Crystal structure and thermal expansion of LuB_{12} single crystals"; *Acta Crystallogr. Sect. A* **56** (Supplement), s421 (2000).
- [19] Hamada, K., Wakata, M., Sugii, N., Matsuura, K., Kubo, K., and Yamauchi, H.; "Phase transition in the $Zr_{1-x}Sc_xB_{12}$ system"; *Phys. Rev. B* **48**, 6892–6898 (1993).
- [20] Paderno, Y. and Shitsevalova, N.; "Stabilization of cubic scandium dodecaboride"; *J. Alloy. Compd.* **219**, 119–123 (1995).
- [21] Kohout, A., Batko, I., Czopnik, A., Flachbart, K., Matas, S., Meissner, M., Paderno, Y., Shitsevalova, N., and Siemensmeyer, K.; "Phase diagram and magnetic structure investigation of the fcc antiferromagnet HoB_{12} "; *Phys. Rev. B* **70**, 224416 (2004).
- [22] Siemensmeyer, K., Flachbart, K., Gabáni, S., Mat'áš, S., Paderno, Y., and Shitsevalova, N.; "Magnetic structure of rare-earth dodecaborides"; *J. Solid State Chem.* **179**, 2748–2750 (2006).
- [23] Siemensmeyer, K., Habicht, K., Lonkai, T., Mat'áš, S., Gabáni, S., Shitsevalova, N., Wulf, E., and Flachbart, K.; "Magnetic properties of the frustrated fcc-antiferromagnet HoB_{12} above and below T_N "; *J. Low Temp. Phys.* **146**, 581–605 (2007).

- [24] Sluchanko, N. E., Azarevich, A. N., Bogach, A. V., Vlasov, I. I., Glushkov, V. V., Demishev, S. V., Maksimov, A. A., Tartakovskii, I. I., Filatov, E. V., Flachbart, K., Gabáni, S., Filippov, V. B., Shitsevalova, N. Y., and Moshchalkov, V. V.; "Effects of disorder and isotopic substitution in the specific heat and Raman scattering in LuB_{12} "; *J. Exp. Theor. Phys.* **113**, 468–482 (2011).
- [25] Sluchanko, N. E., Azarevich, A. N., Bogach, A. V., Gavrilkin, S. Y., Glushkov, V. V., Demishev, S. V., Dukhnenko, A. V., Lyashchenko, A. B., Mitsen, K. V., and Filipov, V. B.; " ^{10}B - ^{11}B isotope substitution and superconductivity in ZrB_{12} "; *JETP Lett.* **94**, 642–646 (2011).
- [26] Sluchanko, N. E., Azarevich, A. N., Bogach, A. V., Glushkov, V. V., Demishev, S. V., Anisimov, M. A., Levchenko, A. V., Filipov, V. B., and Shitsevalova, N. Y.; "Hall and transverse even effects in the vicinity of a quantum critical point in $\text{Tm}_{1-x}\text{Yb}_x\text{B}_{12}$ "; *J. Exp. Theor. Phys.* **115**, 509–526 (2012).
- [27] Sluchanko, N., Bogach, A., Bolotina, N., Glushkov, V., Demishev, S., Dudka, A., Krasnorussky, V., Khrykina, O., Krasikov, K., Mironov, V., Filipov, V. B., and Shitsevalova, N.; "Rattling mode and symmetry lowering resulting from the instability of the B_{12} molecule in LuB_{12} "; *Phys. Rev. B* **97**, 035150 (2018).
- [28] Franz, R. and Werheit, H.; "Jahn-Teller effect of the B_{12} icosahedron and its general influence on the valence band structures of boron-rich solids"; *Europhys. Lett.* **9**, 145–50 (1989).
- [29] Franz, R. and Werheit, H.; "Influence of the Jahn-Teller effect on the electronic band structure of boron-rich solids containing B_{12} icosahedra"; *AIP Conf. Proc.* **231**, 29–36 (1991).
- [30] Bersuker, I. B. and Polinger, V. Z. (eds.); "Vibronic interactions in molecules and crystals"; Springer Series in Chemical Physics vol. 49, (Springer, Berlin, Heidelberg, 1989).
- [31] Gehring, G. A. and Gehring, K. A.; "Co-operative Jahn-Teller effects"; *Rep. Prog. Phys.* **38**, 1–89 (1975).
- [32] Kaplan, M. D. and Vekhter, B. G.; "Cooperative phenomena in Jahn-Teller crystals", (Plenum Press, New York, 1995).
- [33] Bolotina, N. B., Dudka, A. P., Khrykina, O. N., Krasnorussky, V. N., Shitsevalova, N. Y., Filipov, V. B., and Sluchanko, N. E.; "The lower symmetry electron-density distribution and the charge transport anisotropy in cubic dodecaboride LuB_{12} "; *J. Phys.: Condens. Matter* **30**, 265402 (2018).
- [34] Trueblood, K. N., Bürgi, H.-B., Burzlaff, H., Dunitz, J. D., Gramaccioli, C. M., Schulz, H. H., Shmueli, U., and Abrahams, S. C.; "Atomic displacement parameter nomenclature. Report of a subcommittee on atomic displacement parameter nomenclature."; *Acta Crystallogr. Sect. A* **52**, 770–781 (1996).

36 | Chapter 3 Crystal structures of dodecaborides: complexity in simplicity

- [35] Einstein, A.; "Die Plancksche Theorie der Strahlung und die Theorie der spezifischen Wärme"; *Ann. Phys.* **327**, 180–190 (1907).
- [36] Debye, P.; "Vorträge über die kinetische Theorie der Materie und der Elektrizität"; *Mathematische Vorlesungen an der Universität Göttingen*, vol. 6, (B.G. Teubner, Leipzig, 1914).
- [37] Dudka, A. P., Bolotina, N. B., and Khrykina, O. N.; "DebyeFit: a simple tool to obtain an appropriate model of atomic vibrations in solids from atomic displacement parameters obtained at different temperatures"; *J. Appl. Crystallogr.* **52**, 690–692 (2019).
- [38] Bolotina, N. B., Dudka, A. P., Khrykina, O. N., Glushkov, V. V., Azarevich, A. N., Krasnorussky, V. N., Gabáni, S., Shitsevalova, N. Y., Dukhnenko, A. V., Filipov, V. B., and Sluchanko, N. E.; "On the role of isotopic composition in crystal structure, thermal and charge-transport characteristics of dodecaborides $\text{Lu}^{\text{N}}\text{B}_{12}$ with the Jahn-Teller instability"; *J. Phys. Chem. Solids* **129**, 434–441 (2019).
- [39] Korsukova, M.; "Vacancies and thermal vibrations of atoms in the crystal structure of rare earth hexaborides"; *Jpn. J. Appl. Phys. Series* **10**, 15–18 (1994); Proc. 11th Int. Symp. Boron, Borides and Rel. Compd., Tsukuba (Japan), 1993.
- [40] Takahashi, Y., Ohshima, K., Okamura, F. P., Otani, S., and Tanaka, T.; "Crystallographic parameters of atoms in the single crystals of the compounds RB_6 ($R = \text{Y, La, Ce, Nd, Sm, Eu, Gd}$)"; *J. Phys. Soc. Jpn.* **68**, 2304–2309 (1999).
- [41] Trounov, V. A., Malyshev, A. L., Chernyshov, D. Y., Korsukova, M. M., Gurin, V. N., Aslanov, L. A., and Chernyshev, V. V.; "Temperature dependences of the parameters of atoms in the crystal structure of the intermediate-valence semiconductor SmB_6 : investigation by high-resolution powder neutron diffraction"; *J. Phys.: Condens. Matter* **5**, 2479–2488 (1993).
- [42] Trounov, V. A., Malyshev, A. L., Chernyshov, D. Y., Korsukova, M. M., and Gurin, V. N.; "Thermal vibrations and static displacements of atoms in the crystal structure of neodymium and samarium hexaborides"; *Fiz. Tverd. Tela* **36**, 2687–2694 (1994).
- [43] Khrykina, O. N., Dudka, A. P., Bolotina, N. B., Sluchanko, N. E., and Shitsevalova, N. Y.; "Structural instability and poorly defined phase transitions in rare-earth dodecaborides RB_{12} ($R = \text{Ho-Lu}$) at intermediate temperatures"; *Solid State Sci.* **107**, 106273 (2020).
- [44] Kalvius, G. M., Noakes, D. R., Wäppling, R., Kratzer, A., Schreier, E., Iga, F., Takabatake, T., and Löhneysen, H.; " μSR spectroscopy of the Kondo insulators $\text{Lu}_{1-x}\text{Yb}_x\text{B}_{12}$ "; *Physica B: Condens. Matter* **312–313**, 210–212 (2002); the International Conference on Strongly Correlated Electron Systems.
- [45] Kalvius, G. M., Noakes, D. R., Marcano, N., Wäppling, R., Iga, F., and Takabatake, T.; "Dynamics of the internal field in RB_{12} ($R = \text{Er, Yb}$,"

- Lu)”; *Physica B: Condens. Matter* **326**, 398–402 (2003).
- [46] Dudka, A. P., Khrykina, O. N., Bolotina, N. B., and Shitsevalova, N. Y.; “Jahn-Teller lattice distortions and asymmetric electron density distribution in the structure of TmB_{12} dodecaboride in the temperature range of 85–293 K”; *Crystallogr. Rep.* **64**, 737–742 (2019).
- [47] Dudka, A. P., Khrykina, O. N., Bolotina, N. B., Azarevich, A. N., Gavrilkin, S. Y., and Sluchanko, N. E.; “Fine details of the crystal structure and atomic vibrations in YbB_{12} with a metal-insulator phase transition”; in preparation.
- [48] Bolotina, N. B., Verin, I. A., Shitsevalova, N. Y., Filippov, V. B., and Sluchanko, N. E.; “Structural features of single crystals of LuB_{12} upon a transition to the cage-glass phase”; *Crystallogr. Rep.* **61**, 181–186 (2016).
- [49] Dudka, A. P., Khrykina, O. N., Bolotina, N. B., Shitsevalova, N. Y., Filippov, V. B., and Sluchanko, N. E.; “An exceptionally-high diffraction quality dodecaboride LuB_{12} : Growth and single-crystal structure”; *J. Alloy. Compd.* **692**, 535–544 (2017).
- [50] Dudka, A.; “ASTRA—a program package for accurate structure analysis by the intermeasurement minimization method”; *J. Appl. Crystallogr.* **40**, 602–608 (2007).
- [51] Dudka, A.; “New approaches to scaling data measured on a CCD diffractometer”; *J. Appl. Crystallogr.* **43**, 1440–1451 (2010).
- [52] Dudka, A. P.; “ASTRA 4.0 Program: Data reduction for obtaining structure results of extreme accuracy”; *Crystallogr. Rep.* **63**, 1051–1056 (2018).
- [53] Dudka, A. P., Smirnova, E. S., Verin, I. A., and Bolotina, N. B.; “Algorithm and program for precise determination of unit-cell parameters of single crystal taking into account the sample eccentricity”; *Crystallogr. Rep.* **62**, 651–659 (2017).
- [54] Mori, T., Gumeniuk, R., Grin, Y., Vasylechko, L., Dementiy, G., and Shitsevalova, N.; “Thermal expansion and boron isotope effect of LuB_{12} ”; *HASYLAB Annual Report*, pp. 873–874 (2007).
- [55] Gabunia, D., Tsagareishvili, O., Chkhartishvili, L., and Gabunia, L.; “Isotopic composition dependences of lattice constant and thermal expansion of β -rhombohedral boron”; *J. Phys. Conf. Ser.* **176**, 012022 (2009).
- [56] Sluchanko, N. E., Azarevich, A. N., Bogach, A. V., Bolotina, N. B., Glushkov, V. V., Demishev, S. V., Dudka, A. P., Khrykina, O. N., Filippov, V. B., Shitsevalova, N. Y., Komandin, G. A., Muratov, A. V., Aleshchenko, Y. A., Zhukova, E. S., and Gorshunov, B. P.; “Observation of dynamic charge stripes in $\text{Tm}_{0.19}\text{Yb}_{0.81}\text{B}_{12}$ at the metal-insulator transition”; *J. Phys.: Condens. Matter* **31**, 065604 (2019).